JCTC Journal of Chemical Theory and Computation

An Efficient Linear-Scaling Electrostatic Coupling for Treating Periodic Boundary Conditions in QM/MM Simulations

Teodoro Laino,*,† Fawzi Mohamed,‡ Alessandro Laio,‡ and Michele Parrinello‡

Scuola Normale Superiore di Pisa, Piazza dei Cavalieri 7, I-56125 Pisa, Italy, and Computational Science, Department of Chemistry and Applied Biosciences, ETH Zürich, USI Campus, Via Giuseppe Buffi 13, CH-6900 Lugano, Switzerland

Received March 29, 2006

Abstract: A new linear-scaling method based on a multigrid approach to treat long-range electrostatic interactions in hybrid quantum mechanics/molecular mechanics (QM/MM) simulations is described. The scheme has been implemented in the context of a QM calculation based on density functional theory (DFT). The method is tested on an analytical model to validate the new algorithm. Two realistic problems in α-quartz crystals and a zwitterionic dipeptide (GLY-ALA) in water have been chosen as further tests. Results from QM/MM calculations with periodic boundary conditions (PBC) show that the use of PBC is essential when studying highly ordered crystal structures, unless a carefully designed MM crystal is used for the calculation. With a general shaped MM subsystem, the absence of PBC leads to an incorrect description of Kohn−Sham band gaps and charge density. The present method allows periodic boundary conditions to be used in molecular simulations of biological and material science systems.

1. Introduction

Understanding and predicting the properties of condensed systems requires, among other things, the reliable treatment of the long-range Coulomb interactions.[1] Many schemes have been proposed, and a consensus has emerged regarding the use of periodic boundary conditions (PBC) to treat properly the interactions between the periodic replicas. In fact, it is usually believed that PBC have to be used together with an exact treatment of the long-range interactions between the periodically repeated images in order to obtain reliable MD simulations.[2−7]

Although numerous methods have been developed to avoid the truncation of the electrostatic interactions beyond a given cutoff, they have all been applied in the context of classical simulations.[8−13] These methods are all based on different techniques to compute the lattice sum involved in the evaluation of the long-range electrostatic interactions within PBC.

The treatment of long-range forces in conjunction with PBC is much less well established for hybrid quantum mechanics/molecular mechanics (QM/MM) simulations. So far, most of the QM/MM implementations have relied on a spherical truncation scheme, in which the solute(QM)−solvent(MM) electrostatic interactions are neglected beyond a certain cutoff distance R_c. There are only a few exceptions to this implementation. A very popular and inexpensive approach is the reaction field method, which couples the spherical truncation scheme with a polarizable continuum medium that extends beyond a cutoff distance R_c.[14−19] Ewald's lattice summation techniques were also investigated to treat the long-range QM/MM electrostatic interactions. Within a semiempirical framework, the first implementation is due to Gao and Alhambra.[20] In their scheme only the long-range QM/MM interactions are evaluated, while the QM/QM ones are omitted. For the particular set of applications tested by these authors, namely solvation phenomena, the solute−solvent (QM/MM) interactions were considered as the determining ones. Recent implementations of Ewald

* Corresponding author fax: +41919138817; e-mail: teodoro.laino@sns.it.
† Scuola Normale Superiore di Pisa.
‡ ETH Zürich.

10.1021/ct6001169 CCC: $33.50
Published on Web 08/05/2006

techniques extended to the full QM/MM long-range interactions[21,22] show indeed that even for solvation cases long-range QM/QM electrostatic interactions play a significant role. Within a self-consistent DFT scheme, to the best of our knowledge there is only one QM/MM scheme that allows PBC[23] to be used. This approach is conceptually similar to that of the present work, and it relies on the use of splines in reciprocal space (k-space), optimally designed for use within plane wave (PW) codes. The present work[24] is, on the other hand, based on real space techniques and is designed to be used with Gaussian basis codes, as is CP2K.[25]

In a recent paper we proposed a new computational scheme based on the Gaussian expansion of the electrostatic potential (GEEP).[24] This technique can be used efficiently to map functions on a grid, and we applied it to the development of a new QM/MM electrostatic coupling for isolated systems which exhibits linear scaling.

The new scheme, implemented into the CP2K package,[25] extends the recently implemented QM/MM method[24] to applications where the use of PBC is required. It relies on the most efficient methods for calculating long-range electrostatic interactions of point charges within PBC and scales linearly with respect to the number of MM atoms. Moreover the evaluation of the MM electrostatic potential using PBC is independent of the number of QM atoms, depending only on the dimension of the coarsest grid used in the multigrid approach.

An accuracy test was first performed on an analytically solvable model in order to provide a clear and unambiguous validation of the new approach. As a more realistic test case we apply the new method to the study of SiO_2 and its charged oxygen vacancy defect and on a zwitterionic dipeptide (GLY-ALA) in water. The tests show clearly that to achieve a correct description of the QM/MM system there are only two possibilities: the first is based on the optimization of the shape and charges of the MM crystal, to reproduce correctly the long-range stabilizing effects within a truncation scheme,[26] and the other is to treat long-range interactions with a proper PBC scheme. Although results are similar for both approaches the use of QM/MM-PBC schemes avoids the preparation steps related to the fine-tuning of the MM subsystem. For the solvated zwitterionic dipeptide we find, as expected, that the use of QM/MM-PBC can be avoided due to the high dielectric shield and to the lack of long-range stabilizing effects.

2. Methodology

Assuming the overall charge neutrality condition, the total energy of a QM/MM simulation within PBC can be easily evaluated

$$E^{\mathrm{TOT}} = \frac{1}{2}\int\int \mathrm{d}r\mathrm{d}r' \frac{\rho(r)\rho(r')}{|r-r'|} \tag{1}$$

with $\rho = \rho^{\mathrm{QM}} + \rho^{\mathrm{MM}}$ being the total charge density of the system (see Figure 1a). Once the total density is split into a QM and a MM part both subsystems could in principle possess an overall net charge different from zero. Therefore

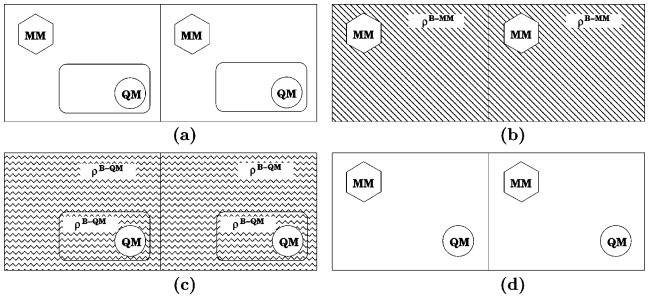

Figure 1. These frames show the decomposition of the total QM/MM energy. In each frame two of the many periodic replica have been shown. Frame (a) shows the total system. Frame (b) shows the energy of the MM subsystem embedded in the neutralizing background charge (deriving from the division of the QM and MM subsystems). Frame (c) shows the energy of the QM subsystem with the neutralizing background charge of the QM cell and that relating to the MM cell. The last frame (see frame (d)) depicts the QM/MM pure electrostatic mutual interaction term.

the use of a neutralizing background charge (ρ^{B}) is necessary to avoid divergence in treating electrostatic within PBC. The total energy term can be split into three separate terms (see Figure 1a):

$$E^{\mathrm{MM}} = \frac{1}{2}\int\int \mathrm{d}r\mathrm{d}r' \frac{(\rho^{\mathrm{MM}}(r)+\rho^{\mathrm{B,MM}})(\rho^{\mathrm{MM}}(r')+\rho^{\mathrm{B,MM}})}{|r-r'|} \tag{2}$$

$$E^{\mathrm{QM}} = \frac{1}{2}\int\int \mathrm{d}r\mathrm{d}r' \frac{(\rho^{\mathrm{QM}}(r)+\rho^{\mathrm{B,QM}})(\rho^{\mathrm{QM}}(r')+\rho^{\mathrm{B,QM}})}{|r-r'|} \tag{3}$$

$$E^{\mathrm{QM/MM}} = \int\int \mathrm{d}r\mathrm{d}r' \frac{(\rho^{\mathrm{QM}}(r)+\rho^{\mathrm{B,QM}})(\rho^{\mathrm{MM}}(r')+\rho^{\mathrm{B,MM}})}{|r-r'|} \tag{4}$$

The physical nature of these terms is illustrated pictorially in Figure 1. Assuming the total charge of the system is zero (although this assumption can be relaxed with no modifications to the formalism) the mixed terms involving the neutralizing background charge of the $E^{\mathrm{QM/MM}}$ cancel the interaction terms of the QM and MM density with their own background charges. The total expression for the three terms is

$$E^{\mathrm{MM}} = \frac{1}{2}\int\int \mathrm{d}r\mathrm{d}r' \frac{(\rho^{\mathrm{MM}}(r))(\rho^{\mathrm{MM}}(r'))}{|r-r'|} \tag{5}$$

$$E^{\mathrm{QM}} = \frac{1}{2}\int\int \mathrm{d}r\mathrm{d}r' \frac{(\rho^{\mathrm{QM}}(r))(\rho^{\mathrm{QM}}(r'))}{|r-r'|} \tag{6}$$

$$E^{\mathrm{QM/MM}} = \int\int \mathrm{d}r\mathrm{d}r' \frac{(\rho^{\mathrm{QM}}(r))(\rho^{\mathrm{MM}}(r'))}{|r-r'|} \tag{7}$$

The first term (Figure 1b) is evaluated using standard techniques such as particle−particle or particle−mesh schemes. The second term (Figure 1c) is the evaluation of the energy of the QM subsystem. Since the total energy of the QM subsystem is usually evaluated exploiting a smaller cell, care needs to be taken to include the correct electrostatic

interactions of the periodic QM replicas. The last term (Figure 1d) is the evaluation of the periodic MM electrostatic potential, partitioned into a real space contribution and a periodic correction. The real space term contains the interaction due to the short-range part of the electrostatic potential of the MM charges with the total quantum charge distribution (electrons plus nuclei). Only MM atoms close to the QM region will contribute to this term. The periodic term contains instead the long-range effects of the MM subsystem.

In the next section, the standard Ewald method is briefly revised for a N-point charge particle system interacting in an orthorhombic box of edge L_x, L_y, L_z. Particular care is then devoted to the discussion of the use of the Ewald lattice summation with the GEEP scheme.[24] Finally we discuss the algorithm to decouple/recouple multiple QM images. In the following Latin letters a and b will be used to index the MM atoms, while Greek letters α and β will be used for QM atoms.

2.1. Ewald Lattice Summation for Electrostatic Interactions. Given an N-point charge particle system, the electrostatic potential $\Phi_{tot}(\mathbf{r})$ at position $\mathbf{r}$ is evaluated using the Ewald lattice sum technique.[8] In this approach, $\Phi_{tot}(\mathbf{r})$ is split into the sum of two potentials, using a Gaussian screening charge of width κ:

$$\Phi_{tot}(\mathbf{r}) = \Phi_{rec}(\mathbf{r}) + \Phi_{real}(\mathbf{r}) \tag{8}$$

The reciprocal space potential term $\Phi_{rec}(\mathbf{r})$ can be determined using the Fourier series

$$\Phi_{rec}(\mathbf{r}) = \frac{4\pi}{V}\sum_{\mathbf{k}\neq 0}\frac{e^{-k^2/4\kappa}}{k^2}\sum_{a}^{MM} q_a e^{-i\mathbf{k}\cdot|\mathbf{r}-\mathbf{r}_a|} \tag{9}$$

where $\mathbf{k} = [2\pi n_x/L_x^2, 2\pi n_y/L_y^2, 2\pi n_z/L_z^2]$, and V is the volume of the primary unit cell. The real space part of the Ewald potential is given by

$$\Phi_{real}(\mathbf{r}) = \sum_{a}^{MM}\sum_{|\mathbf{L}|\leq L_{cut}} q_a \frac{\mathrm{Erfc}(\kappa|\mathbf{r}-\mathbf{r}_a+\mathbf{L}|)}{|\mathbf{r}-\mathbf{r}_a+\mathbf{L}|} \tag{10}$$

where $\mathbf{L} = [n_x L_x, n_y L_y, n_z L_z]$ counts the periodic images with n_k integers. As the Erfc has a real space short-range property, only the $|\mathbf{L}| \leq L_{cut}$ periodic images will contribute to the real space term of the electrostatic potential.

2.2. GEEP. The evaluation of a scalar field on grids can be efficiently achieved by exploiting the recently proposed technique of the Gaussian expansion of the electrostatic potential, namely GEEP,[24] that we applied to the evaluation of the QM/MM electrostatic potential. Following ref 24, the charge on MM atoms is represented with a Gaussian distribution

$$\rho(|\mathbf{r}-\mathbf{r}_a|) = \left(\frac{1}{\sqrt{\pi} r_{c,a}}\right)^3 \exp\left(-\frac{|\mathbf{r}-\mathbf{r}_a|^2}{r_{c,a}^2}\right) \tag{11}$$

where $r_{c,a}$ is the width of the Gaussian charge of the classical atom a. An accurate analysis of the use of nonpointlike atomic potentials in QM/MM simulations has recently been published.[27] The electrostatic potential originated by the Gaussian charge distribution can be evaluated analytically:

$$v_a(\mathbf{r},\mathbf{r}_a) = \frac{\mathrm{Erf}(|\mathbf{r}-\mathbf{r}_a|/r_{c,a})}{|\mathbf{r}-\mathbf{r}_a|} \tag{12}$$

Using GEEP we can write this potential energy function as a series of short-range functions plus a residual function with a very low cutoff:

$$v_a(\mathbf{r},\mathbf{r}_a) = \frac{\mathrm{Erf}(|\mathbf{r}-\mathbf{r}_a|/r_{c,a})}{|\mathbf{r}-\mathbf{r}_a|} = \sum_{N_g} A_g \exp\left(-\frac{|\mathbf{r}-\mathbf{r}_a|^2}{G_g^2}\right) + R_{low}(|\mathbf{r}-\mathbf{r}_a|) \tag{13}$$

The smoothed Coulomb potential is then expressed as a sum of N_g Gaussian functions and of a residual function R_{low}. The A_g are the amplitudes of the Gaussian functions, G_g their width. The Gaussian functions will be mapped on grids and their contribution neglected if their value is less than a preassigned threshold. This is equivalent to assuming that Gaussians are compact support functions, namely that they are numerically zero beyond a certain distance from the MM atom on which the Gaussian is centered. If the parameters A_g and G_g are properly chosen, the residual function R_{low} is smooth, i.e., its Fourier transform is approximately zero for $|\mathbf{k}| \gg k_{cut}$. The k_{cut} parameter is related to the spacing of the grid on which the R_{low} function will be mapped. Within a multigrid framework this implies that a good representation of the function is obtained on a coarse grid, chosen in order to have the same grid cutoff as the cutoff of the residual function.

It can be easily shown that the evaluation of the electrostatic potential scales linearly for systems as small as hundreds of atoms, with a prefactor which depends only on the number of grid points of the coarsest grid level.[24]

2.3. QM/MM Periodic Potential. The QM/MM periodic potential (see Figure 1d) on a generic point i of the finest grid level can be computed using the real space lattice sum

$$V^{fine}(\mathbf{r}_a)_i = \sum_{a}^{MM}\sum_{\mathbf{L}}^{\infty}{}' q_a v_a(\mathbf{r}_i,\mathbf{r}_a+\mathbf{L}) \tag{14}$$

where $\mathbf{r}_i$ is the coordinate of the point i of the finest grid level and $\mathbf{r}_a$ indexes the functional dependence from the set of MM atomic coordinates. The summation over $\mathbf{L}$ involves all integer translations of the real space lattice vectors $\mathbf{L} = [n_x L_x, n_y L_y, n_z L_z]$ for integers n_k, and the prime symbol indicates that when $\mathbf{L} = 0$ the term $|\mathbf{r}_i - \mathbf{r}_a| = 0$ is neglected. $v_a(\mathbf{r}_i,\mathbf{r}_a+\mathbf{L})$ represents the functional form of the electrostatic potential. The summation in eq 14 has the same convergency properties as the standard Ewald summation schemes.[8]

The total QM/MM electrostatic energy can be split into two rapidly convergent terms,[8,28] one over real space and the other over reciprocal space lattice vectors

$$E^{QM/MM}(\mathbf{r}_\alpha,\mathbf{r}_a) = E^{QM/MM}_{real}(\mathbf{r}_\alpha,\mathbf{r}_a) + E^{QM/MM}_{recip}(\mathbf{r}_\alpha,\mathbf{r}_a) \tag{15}$$

where

$$E_{\text{real}}^{\text{QM/MM}}(\mathbf{r}_\alpha,\mathbf{r}_a) = \int d\mathbf{r}\rho(\mathbf{r},\mathbf{r}_\alpha)V_{\text{real}}^{\text{QM/MM}}(\mathbf{r},\mathbf{r}_a) \quad (16)$$

and

$$E_{\text{recip}}^{\text{QM/MM}}(\mathbf{r}_\alpha,\mathbf{r}_a) = \int d\mathbf{r}\rho(\mathbf{r},\mathbf{r}_\alpha)V_{\text{recip}}^{\text{QM/MM}}(\mathbf{r},\mathbf{r}_a) \quad (17)$$

The definition of the two terms is strictly connected to the type of functional form used to describe the Coulomb interactions. In our case, since we decided to treat the MM classical charges through a Gaussian charge distribution, the electrostatic potential function has the analytical form

$$v_a(\mathbf{r},\mathbf{r}_a) = \frac{\text{Erf}(|\mathbf{r}-\mathbf{r}_a|/r_{c,a})}{|\mathbf{r}-\mathbf{r}_a|} \quad (18)$$

easily represented as a sum of two terms:[24]

$$v_a(\mathbf{r},\mathbf{r}_a) = \frac{\text{Erf}(|\mathbf{r}-\mathbf{r}_a|/r_{c,a})}{|\mathbf{r}-\mathbf{r}_a|} = \sum_{N_g} A_g \exp\left(-\frac{|\mathbf{r}-\mathbf{r}_a|^2}{G_g^{\,2}}\right) + R_{\text{low}}(|\mathbf{r}-\mathbf{r}_a|) \quad (19)$$

The best choice is to use the mathematical properties of the two functional forms (short-range term and long-range term) to define the division into real and reciprocal space contributions:

$$v_a(\mathbf{r},\mathbf{r}_a) = \frac{\text{Erf}(|\mathbf{r}-\mathbf{r}_a|/r_{c,a})}{|\mathbf{r}-\mathbf{r}_a|} = \sum_{N_g} A_g \exp\left(-\frac{|\mathbf{r}-\mathbf{r}_a|^2}{G_g^{\,2}}\right) + R_{\text{low}}(|\mathbf{r}-\mathbf{r}_a|) \quad (20)$$

$$= v_a^{rs}(\mathbf{r},\mathbf{r}_a) + v_a^{\text{recip}}(\mathbf{r},\mathbf{r}_a) \quad (21)$$

All short-range interactions will be evaluated in the real space, while all long-range interactions will be taken into account in the reciprocal space formalism.

The real space term $V_{\text{real}}^{\text{QM/MM}}(\mathbf{r},\mathbf{r}_a)$ is defined as

$$V_{\text{real}}^{\text{QM/MM}}(\mathbf{r},\mathbf{r}_a) = \sum_{|\mathbf{L}| \le L_{\text{cut}}} \sum_a q_a v_a^{rs}(\mathbf{r},\mathbf{r}_a+\mathbf{L}) = \sum_{|\mathbf{L}| \le L_{\text{cut}}} \sum_a q_a \left[\sum_{N_g} A_g \exp\left(-\frac{|\mathbf{r}-\mathbf{r}_a+\mathbf{L}|^2}{G_g^{\,2}}\right)\right] \quad (22)$$

where a labels the MM atoms. The radii of the Gaussians are such that only a few periodic images ($|\mathbf{L}| \le L_{\text{cut}}$) are needed to achieve convergence of the real space term, while others give zero contribution. As in ref 24, each Gaussian of eq 22 is mapped on the appropriate grid level.

The effect of the periodic replicas of the MM subsystem is only in the long-range term, and it comes entirely from the residual function $R_{\text{low}}(\mathbf{r},\mathbf{r}_a)$ of eq 20:

$$V_{\text{recip}}^{\text{QM/MM}}(\mathbf{r},\mathbf{r}_a) = \sum_{\mathbf{L}}^{\infty}{}' \sum_a q_a v_a^{\text{recip}} = \sum_{\mathbf{L}}^{\infty}{}' \sum_a q_a R_{\text{low}}(|\mathbf{r}-\mathbf{r}_a+\mathbf{L}|) \quad (23)$$

Performing the same manipulation used in Ewald summation[8] (see Appendix B) the previous equation can be computed more efficiently in the reciprocal space:

$$V_{\text{recip}}^{\text{QM/MM}}(\mathbf{r}_i,\mathbf{r}_a) = L^{-3} \sum_{\mathbf{k}}^{k_{\text{cut}}}{}' \sum_a \tilde{R}_{\text{low}}(\mathbf{k}) q_a \cos[2\pi\mathbf{k}\cdot(\mathbf{r}_i-\mathbf{r}_a)] \quad (24)$$

The term $\tilde{R}_{\text{low}}(\mathbf{k})$, representing the Fourier transform of the smooth electrostatic potential, can be evaluated analytically:

$$\tilde{R}_{\text{low}}(\mathbf{k}) = \left[\frac{4\pi}{|\mathbf{k}|^2}\right] \exp\left(-\frac{|\mathbf{k}|^2 r_{c,a}^{\,2}}{4}\right) - \sum_{N_g} A_g (\pi)^{3/2} G_g^{\,3} \exp\left(-\frac{G_g^{\,2}|\mathbf{k}|^2}{4}\right) \quad (25)$$

The potential in eq 24 can be mapped on the coarsest grid. In fact, the long-range contribution is physically very smooth, and a good representation can be achieved with large grid spacings. Furthermore, since the R_{low} function is a low cutoff function, $\tilde{R}_{\text{low}}(\mathbf{k})$ is zero for all $\mathbf{k}$-vectors larger than a well defined k_{cut}. The k_{cut} parameter depends strongly on the number of Gaussian functions used in the GEEP scheme (as described in ref 24).

Once the electrostatic potential of a single MM charge within periodic boundary conditions is derived, the evaluation of the electrostatic potential due to the MM subsystem is easily computed employing the same multigrid operators (interpolation and restriction) described in ref 24.

2.4. Periodic Coupling with QM Images. In the present section we complete the description of the electrostatic coupling, discussing the interaction between the periodic images of the QM replicas (see Figure 1c). The Quickstep[29,30] algorithm uses a mixed plane wave/Gaussian basis set to solve the DFT equations for the quantum subsystem. The plane waves are used to compute efficiently the Hartree potential. Therefore, unless the quantum box and the MM box have the same dimensions, the QM images, interacting by PBC implicit in the evaluation of the Hartree potential, have the wrong periodicity.

To avoid this error, the QM problem is usually solved using standard decoupling techniques.[31,32] This approximation is legitimate when the evaluation of the QM/MM potential is performed using spherical truncation schemes for Coulomb interactions.

Since we want to describe the long-range QM/MM interaction with periodic boundary conditions, we may not neglect the QM/QM periodic interactions, which play a significant role if the QM subsystem has a net charge different from zero or a significant dipole moment. Therefore we exploit a technique recently proposed by Blöchl,[32] which decouples the periodic images in order to restore the correct periodicity also for the QM part. A full and comprehensive description of the methods to evaluate energy corrections and derivatives is given in ref 32. Here we summarize Blöchl's decoupling scheme. Given a QM total density charge $\rho(\mathbf{r},\mathbf{r}_\alpha)$, the electrostatic energy of this

isolated density is

$$E = \frac{1}{2}\int_V \mathrm{d}\mathbf{r} \int \mathrm{d}\mathbf{r}' \frac{\rho(\mathbf{r},\mathbf{r}_\alpha)\rho(\mathbf{r}',\mathbf{r}_\alpha)}{|\mathbf{r}-\mathbf{r}'|} \tag{26}$$

Let us introduce a new model charge density $\hat{\rho}(\mathbf{r},\mathbf{r}_\alpha)$, which is localized within the same volume V as $\rho(\mathbf{r},\mathbf{r}_\alpha)$ and which reproduces the multipole moments of the correct charge distribution. The representation adopted in ref 32 is given as a sum

$$\hat{\rho}(\mathbf{r},\mathbf{r}_\alpha) = \sum_\alpha q_\alpha g_\alpha(\mathbf{r},\mathbf{r}_\alpha) \tag{27}$$

of atom-centered spherical Gaussians, which are normalized such that they possess a charge of one

$$g_i(\mathbf{r},\mathbf{r}_\alpha) = \frac{1}{(\sqrt{\pi}r_{c,\alpha})^3}\exp\left(-\frac{|\mathbf{r}-\mathbf{r}_\alpha|^2}{r_{c,\alpha}{}^2}\right) \tag{28}$$

where $\mathbf{r}_\alpha$ denotes a particular atomic site. Every atomic site may be the center of various Gaussians with different decay lengths $r_{c,\alpha}$. By construction, the multipole moments of the model charge density agree with those of the original charge distribution. Since the electrostatic interaction of separated charge distribution (the array of periodic QM charge densities) depends only on its multipole moments, the model charge density is used to modify the Hartree potential and to cancel the electrostatic interactions between the periodic images. In Appendix A, we briefly summarize with a matrix formalism the charge fit scheme as derived in ref 32. In the same way that the Blöchl scheme cancels the electrostatic interactions between periodic images, it is possible to use it to include the electrostatic interactions between periodic images with the periodicity of the MM box.

2.5. QM/MM Forces. The derivatives on MM atoms can be easily evaluated taking the derivative of both terms in real space and in reciprocal space and summing the contribution of the different grid levels. The derivatives of the real space term are the same as the one presented in ref 24. The derivatives of the reciprocal space term need to be evaluated by deriving the MM nuclei potential energy contribution and integrating this derivative with the quantum charge distribution

$$\frac{\partial E_{\mathrm{recip}}^{\mathrm{QM/MM}}(\mathbf{r}_\alpha,\mathbf{r}_a)}{\partial \mathbf{r}_a} = \int d\mathbf{r}\rho(\mathbf{r},\mathbf{r}_\alpha)\frac{\partial V_{\mathrm{recip}}^{\mathrm{QM/MM}}(\mathbf{r},\mathbf{r}_a,\mathbf{r}_\alpha)}{\partial \mathbf{r}_a} = \tag{29}$$

$$\Delta\omega\sum_{\mathbf{r}_i}\rho(\mathbf{r}_i,\mathbf{r}_\alpha)L^{-3}\sum_{\mathbf{k}}^{k_{\mathrm{cut}}}{}'\sum_{a}^{\mathrm{MM}}\tilde{R}_{\mathrm{low}}(\mathbf{k})q_a\frac{\partial\cos[2\pi\mathbf{k}\cdot(\mathbf{r}_i-\mathbf{r}_a)]}{\partial \mathbf{r}_a} \tag{30}$$

where $\Delta\omega$ is the volume element of the coarsest grid level. This contribution is summed with the terms in real space to obtain the total derivatives on MM atoms. The derivatives on QM atoms are computed in the same way as we described in ref 24, the only difference being that the QM derivatives are modified by the coupling/decoupling terms. These corrections have been derived and extensively discussed in ref 32.

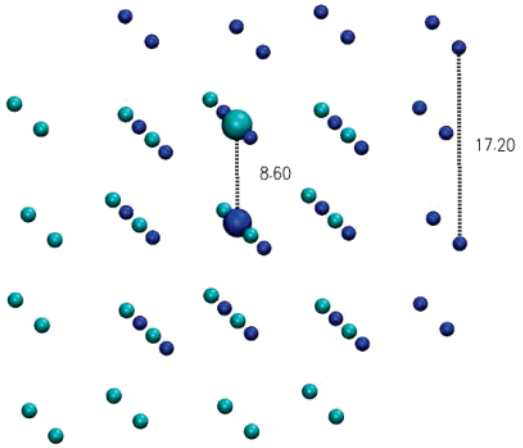

Figure 2. Orthorhombic cell of face centered cubic lattice of Gaussian charges. The two big spheres represent the QM atoms. Lattice parameter 17.2 Å. The Gaussian charges have a width of $0.5\sqrt{2}$ Å.

3. Tests and Applications

Four systems were selected to test the new method. The first one, an infinite array of Gaussian alternating opposite charges, can be solved analytically and therefore provides a clear and unambiguous test of the accuracy of our new approach.

The second system is a periodic model of α-quartz (α-SiO_2) where a bulk fragment, described at the DFT level, is embedded in the environment of classical atoms described with MM force fields. The third system analyzes a charged oxygen vacancy defect in α-quartz, in the same periodic model. These two systems do not possess an analytical solution but both have been extensively studied experimentally[33−40] and theoretically.[41−49]

The last system is a zwitterionic dipeptide (GLY-ALA) in water. It was chosen since it represents an extreme test where the use of PBC is expected to have minor effects on the electronic structure properties.

3.1. Analytical Test. To validate this new algorithm, let us consider a simple Gaussian charge distribution

$$\rho(\mathbf{r}_\alpha) = (\kappa/\pi)^{3/2}\exp(-\kappa^2|\mathbf{r}_\alpha|^2) \tag{31}$$

with κ being the width of the Gaussian charge density. Using this system we test and show that for a suitable choice of parameters the results can be made arbitrarily close to the analytical results.

We consider an ordered array of 64 Gaussian charges of alternating signs (32 positively charged (+1) and 32 negatively charged (−1)) arranged to form a NaCl lattice. The potential generated by such a set of charges can be calculated exactly by noting that the electrostatic potential of this charge density at an arbitrary distance $\mathbf{r}$ can be determined analytically, $V_{\mathrm{ext}}(\mathbf{r}) = \mathrm{Erf}(\kappa\mathbf{r})/\mathbf{r}$. We select two neighboring charges (see Figure 2) and calculate the Hartree potential in a smaller orthorhombic cell centered around the two chosen charges. This calculation would have been a necessary step had we treated the two selected centers quantum mechanically instead of with a fixed nuclear charge distribution. The

Table 1: Interaction of a Gaussian Charge Distribution in a 3-Dimensional Lattice as Shown in Figure 2 as a Function of the Number of Gaussians Used in GEEP and as a Function of the QM Cell

QM cell (*x*,*y*,*z*) (Å)	no. of Gaussians	k_{cut} (bohr^{-1})	E_{tot} (Hartree)	ΔE (mHartree)
34.4 34.4 34.4	analytical calculation		3.441010	
34.4 34.4 34.4	6	0.5	3.440520	0.49
34.4 34.4 34.4	6	0.7	3.441176	−0.17
34.4 34.4 34.4	6	1.0	3.441119	−0.11
34.4 34.4 34.4	6	2.0	3.441070	−0.06
34.4 34.4 34.4	6	0.5	3.440520	0.49
34.4 34.4 34.4	9	0.5	3.440687	0.33
34.4 34.4 34.4	12	0.5	3.440885	0.12
34.4 34.4 34.4	15	0.5	3.440895	0.11
34.4 34.4 34.4	15	0.5	3.440895	0.11
27.0 27.0 27.0	15	0.5	3.440978	0.03
34.4 27.0 27.0	15	0.5	3.440951	0.06
22.0 22.0 12.0	15	0.5	3.440865	0.14
12.0 12.0 12.0	15	0.5	3.441356	−0.35
34.4 34.4 34.4	QM/MM nonperiodic[a]		3.443106	2.10

[a] The QM/MM nonperiodic calculation was performed with 64 000 MM atoms arranged in a cube cell of 344.0 Å.

calculation was performed using a plane wave cutoff of 25 Ry, and 3 Gaussians were used for each selected atom to build the model density used to decouple/recouple the periodic images.

In Table 1 we show how this pseudo QM/MM calculation depends on parameters such as the QM cell dimension (affecting the coupling/decoupling between QM periodic images), the k_{cut} parameter of eq 24, and the number of Gaussians used in the GEEP scheme. In particular we note that the number of Gaussians is strictly correlated to the k_{cut} value. In fact, the more Gaussians that are used in the GEEP scheme, the more the R_{low} will be a low cutoff function. This permits a smaller k_{cut} parameter to be used in order to reach the same accuracy (see Table 1).

The choice of the dimension of the QM box is almost irrelevant for the accuracy of the results (see Table 1). In fact even using a box of 12.0 Å, which is the smallest possible box size usable with this QM subsystem, we find accurate results. We remark that other decoupling techniques[23,31] require boxes twice the size of the minimum box, leading to a substantial computational overhead.

Moreover we computed the pseudo QM/MM interaction energy for the nonperiodic pseudo QM/MM calculation, using an MM environment of 64 000 atoms (MM cell side of 344.0 Å). The result shows that for ordered structures surface effects are very important, and the only way to include correctly the electrostatic interactions is by using PBC. Overall this test indicates that the new proposed scheme is both valid and efficient. In terms of computational time no additional overhead was noted when performing pseudo QM/MM calculation with or without PBC.

3.2. SiO_2. We now consider a realistic problem, a crystal of α-SiO_2 (α-quartz) in an orthorhombic cell, subject to periodic boundary conditions. Several QM/MM schemes have been proposed in the literature for silica-based systems,[26,50−56] differing in the description of the quantum-classical interface and of the classical region. All of them treat the QM/MM long-range interaction with a truncation scheme, properly optimizing the charges of the H-atoms terminating the MM cluster or its shape in order to recover the correct long-range effects.

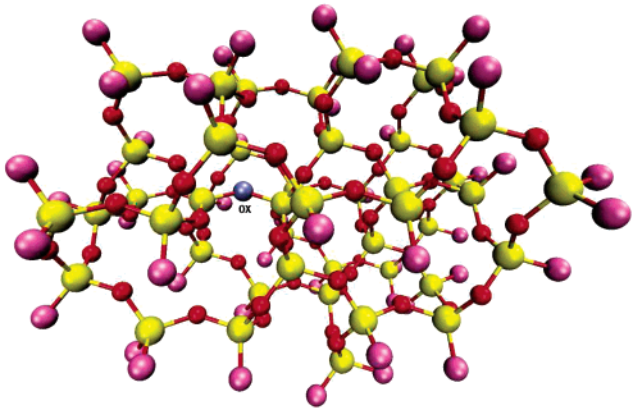

Figure 3. The picture shows the QM cluster. Silicon atoms in yellow, oxygen in red, boundary oxygen atoms (treated increasing the core charge by 0.4) in purple, and in blue the oxygen atom (OX) removed to create the oxygen vacancy defect.

The MM crystal we used for this test is made up of 15 552 atoms (5184 SiO_2 units) in an orthorhombic cell of 49.94, 57.66, and 63.49 Å. The system was optimized using the empirical pair potential of van Beest[57] which is known to provide a reliable description of bulk α-SiO_2.[58] A fragment of 160 atoms was described at the QM level Figure 3, describing the oxygen boundary atoms with a core charge increased by 0.4 in order to maintain the neutrality of the overall system. This boundary scheme has been extensively tested in a recent publication.[26] DFT calculations with Gödecker-Tetter-Hutter (GTH)[59] pseudopotentials[59] using local density approximation to describe the exchange-correlation functional were performed on the QM site using a cutoff of 200 Ry. We optimized the wave function with and without the use of periodic boundary conditions. The results show that the use of periodicity is essential to treat highly ordered crystal structures. Without periodic boundary conditions we find the Kohn−Sham gap to be 0.12 eV which is much lower than the experimental band gap of about 9 eV[60,61] and even than the computed Kohn−Sham gap of 5.8 eV.[42] Also the population analysis gives us an indication that the lack of PBC leads to an incorrect description of the system. In fact by population analysis[32] we find that many oxygen atoms have a positive charge, while some silicon atoms have a negative charge. If we use periodic boundary conditions, on the other hand, we find results that agree with those previously published. In particular, using PBC, we find for the Kohn−Sham band gap a value of 6.23 eV using the same computational parameters as in the case of non-PBC. The population analysis shows the proper charge distribution with charges close to + 2.0 and −1.0 for silicon and oxygen, respectively.

After removing the atom depicted in Figure 3 from the same crystal structure, we studied the charged oxygen vacancy defect in SiO_2 with the same computational setup

used for stoichiometric SiO_2. As for quartz the lack of PBC leads to an incorrect description for both the electronic structure and the population analysis. The use of the present scheme gives a Kohn−Sham band gap of 3.18 eV, as against the theoretical result[42] of 3.30 eV. The value obtained without PBC is 0.0089 eV. Unlike the other QM/MM schemes used for silica we do not use any additional charge to terminate the MM cluster, and no particular attention was paid to the choice of its shape. The computational cost for the evaluation of the QM/MM-PBC electrostatic potential on this system accounts for 5% of the total CPU time of a single MD step. In particular 1 MD step (energy and forces), on Cray-XT3 using 32 processors, requires 7 min. Twenty-three seconds out of 7 min are used to evaluate the QM/MM electrostatic potential. Without using the long-range PBC option the computational time used for the construction of the QM/MM electrostatic potential is roughly 12 s. Thus, the use of PBC does not represent a significant overhead in the overall computation scheme, making feasible the study of crystal structures within a QM/MM-PBC framework.

4. GLY-ALA

The results obtained for SiO_2 both with and without PBC could in principle be attributed to the peculiar electronic structure of this material (with a partial ionic/covalent structure). Therefore we further tested both QM/MM schemes, with and without PBC, on a zwitterionic dipeptide (GLY-ALA) in water, where the long-range stabilizing effects due to the Madelung potential are not present. We expect small effects from using PBC with this particular system.

Using the same description for the QM system as the one previously published,[24] we find that PBC do not affect the value of the Kohn−Sham gap or the charge population analysis with respect to the common implementations where a truncation scheme was used. This is to be expected due to the large dielectric constant of water and to the lack of long-range stabilizing effects such as the Madelung potential in an ionic crystal.

5. Conclusions

A new scheme has been designed to include the effects of periodic boundary conditions into hybrid QM/MM descriptions of chemical/biological systems. The present scheme uses the recently proposed Gaussian expansion of the electrostatic potential (GEEP)[24] and is implemented in the CP2K package.[25] Through the use of a modified Ewald lattice summation it is possible to include the effects of the periodic boundary conditions in the evaluation of the MM electrostatic potential. The scheme preserves the linear-scaling property of the GEEP technique and is computationally efficient. The method has no additional overhead with respect to the evaluation of the QM/MM electrostatic potential with a truncation scheme using a spherical cutoff. The new scheme is validated with an analytical model and with three real test cases: the α-quartz crystal and its charged oxygen vacancy defect and a zwitterionic dipeptide (GLY-ALA) in water. It is clear from these tests that the use of periodic boundary conditions together with proper treatment of the long-range interactions is required for ordered systems, unless a careful truncation scheme optimizing the shape and dipole of the MM environment is used. Therefore, it is now possible to perform routinely ab initio molecular dynamics and electronic structure calculations in crystal systems. The scheme has been developed describing the electrons with DFT, but the extension to other quantum chemical schemes (Hartree−Fock and post Hartree−Fock methods) is straightforward.

Acknowledgment. The authors wish to thank F. Zipoli and D. Donadio for useful discussions regarding the treatment of the silica system.

Appendix A. Construction of the Model Charge Density

The model density $\hat{\rho}(\mathbf{r},\mathbf{r}_\alpha)$ can be derived by minimizing the multipole moments and the net charge of the system:

$$\Delta Q_L = \left|\int \mathrm{d}\mathbf{r}\mathbf{r}^l Y_l(\mathbf{r})(\rho(\mathbf{r},\mathbf{r}_\alpha) - \hat{\rho}(\mathbf{r},\mathbf{r}_\alpha))\right| \quad (32)$$

$$\Delta W = \left|\int \mathrm{d}\mathbf{r}\mathbf{r}^2(\rho(\mathbf{r},\mathbf{r}_\alpha) - \hat{\rho}(\mathbf{r},\mathbf{r}_\alpha))\right| \quad (33)$$

The parameters of the model density are obtained from a fit to the original charge density, which is biased by a weight function. In the reciprocal space, both requirements eqs 32 and 33 can be translated into expressions that are sensitive only to the intermediate neighborhood of the origin. Thus the fit uses a weighting function of the form

$$w(\mathbf{k}) = 4\pi\frac{(|\mathbf{k}|^2 - |\mathbf{k}_{\mathrm{cut}}|^2)^2}{|\mathbf{k}|^2|\mathbf{k}_{\mathrm{cut}}|^2} \quad (34)$$

for $|\mathbf{k}| < |\mathbf{k}_{\mathrm{cut}}|$ and zero elsewhere. The weight function enhances the importance of the low $\mathbf{k}$-vectors while ignoring the high $\mathbf{k}$-vectors of the density.

Using the method of Lagrange multipliers, the parameters of the model density q_α are obtained from the extremal condition of

$$\mathcal{L}(q_\alpha,\lambda) = \frac{V}{2}\sum_{\mathbf{k}\neq 0} w(\mathbf{k})|\rho(\mathbf{k}) - \sum_\alpha q_\alpha g_\alpha(\mathbf{k})|^2 - \lambda V[\rho(\mathbf{k}=0) - \sum_\alpha q_\alpha g_\alpha(\mathbf{k}=0)] \quad (35)$$

In matrix form the equation can be written in

$$\mathbf{Aq} + \lambda\mathbf{C} = \mathbf{BCq} = N \quad (36)$$

where the matrix elements of $\mathbf{A}$, $\mathbf{C}$, and $\mathbf{B}$ are given by

$$A_{i,j} = V\sum_{\mathbf{k}\neq 0} w(\mathbf{k})[g_i^\dagger(\mathbf{k})g_j(\mathbf{k})] \quad (37)$$

$$C_i = Vg_i(\mathbf{k}=0) = 1 \quad (38)$$

$$B_i = V\sum_{\mathbf{k}\neq 0} w(\mathbf{k})Re[\rho^\dagger(\mathbf{k})g_i(\mathbf{k})] \quad (39)$$

and $\mathbf{q}$ is the array of parameters of the model charge density. The solution to this linear equation system is given by

$$\mathbf{q} = \mathbf{A}^{-1}\left[\mathbf{B} - \mathbf{C}\frac{\mathbf{CA}^{-1}\mathbf{B} - N}{\mathbf{CA}^{-1}\mathbf{C}}\right] \quad (40)$$

Appendix B. Derivation of the Long-Range QM/MM Potential

The effect of the periodic copies of the MM subsystem is only in the long-range term, and it comes entirely from the residual function $R_{low}(\mathbf{r},\mathbf{r}_a)$ of eq 20:

$$V_{recip}^{QM/MM}(\mathbf{r},\mathbf{r}_a) = \sum_{\mathbf{L}}^{\infty}{}'\sum_a v_a^{recip} = \sum_{\mathbf{L}}^{\infty}{}'\sum_a R_{low}(|\mathbf{r}-\mathbf{r}_a+\mathbf{L}|) \tag{41}$$

This summation has the same convergence properties as the Ewald series and can be efficiently computed in the reciprocal space. To derive the expression of this modified Ewald sum, let us assume we know the analytical expression of the density $\sigma(\mathbf{r},\mathbf{r}_a)$ originating from the atomic potential R_{low}. The potential at point $\mathbf{r}_i$ due to the charge distribution $\sigma(\mathbf{r},\mathbf{r}_a)$ is

$$V_{recip}^{QM/MM}(\mathbf{r}_i,\mathbf{r}_a) = \int d\mathbf{r}\frac{\sigma(\mathbf{r}+\mathbf{r}_i,\mathbf{r}_a)}{\mathbf{r}} = L^{-3}\int d\mathbf{r}\sum_{\mathbf{k}}^{k_{cut}}{}'\frac{\tilde{\sigma}(\mathbf{k})\exp[-\Delta 2\pi\mathbf{k}(\mathbf{r}+\mathbf{r}_i-\mathbf{r}_a)]}{\mathbf{r}} \tag{42}$$

The use of the identity[62]

$$\int d\mathbf{r}\frac{\exp[-\Delta 2\pi\mathbf{k}(\mathbf{r}+\mathbf{r}_i-\mathbf{r}_a)]}{\mathbf{r}} = \int_0^\infty r dr\int_0^{2\pi}d\phi\int_0^{\pi}\sin\theta d\theta\exp[-\Delta 2\pi|\mathbf{k}||\mathbf{r}+\mathbf{r}_i-\mathbf{r}_a|\cos\theta] \tag{43}$$

$$= \frac{4\pi}{k^2}\cos[2\pi\mathbf{k}\cdot(\mathbf{r}_i-\mathbf{r}_a)] \tag{44}$$

in eq 42 leads to

$$V_{recip}^{QM/MM}(\mathbf{r}_i,\mathbf{r}_a) = 4\pi L^{-3}\sum_{\mathbf{k}}^{k_{cut}}{}'\frac{\tilde{\sigma}(\mathbf{k})}{k^2}\cos[2\pi\mathbf{k}\cdot(\mathbf{r}_i-\mathbf{r}_a)] \tag{45}$$

Using the Maxwell equation $\nabla^2 V = 4\pi\rho$ and its representation in Fourier space, the term in eq 45

$$4\pi\frac{\tilde{\sigma}(\mathbf{k})}{k^2} = \tilde{R}_{low}(\mathbf{k}) \tag{46}$$

is the Fourier transform of the potential originated by the density of charge $\sigma(\mathbf{r},\mathbf{r}_a)$. Then the previous equation can be written as

$$V_{recip}^{QM/MM}(\mathbf{r}_i,\mathbf{r}_a) = L^{-3}\sum_{\mathbf{k}}^{k_{cut}}{}'\sum_a\tilde{R}_{low}(\mathbf{k})q_a\cos[2\pi\mathbf{k}\cdot(\mathbf{r}_i-\mathbf{r}_a)] \tag{47}$$

References

(1) Sagui, C.; Darden, A. *Ann. Rev. Biophys. Biomol. Struct.* **1999**, *28*, 155−179.

(2) Resat, H.; McCammon, J. A. *J. Chem. Phys.* **1996**, *104*, 7645−7651.

(3) Buono, G. S. D.; Cohen, T. S.; Rossky, P. J. *J. Mol. Liq.* **1994**, *60*, 221−236.

(4) Resat, H. *J. Chem. Phys.* **1999**, *110*, 6887−6889.

(5) Rozanska, X.; Chipot, C. *J. Chem. Phys.* **2000**, *112*, 9691−9694.

(6) Brunsteiner, M.; Boresch, S. *J. Chem. Phys.* **2000**, *112*, 6953−6955.

(7) York, D. M.; Darden, T. A.; Pedersen, L. G. *J. Chem. Phys.* **1993**, *99*, 8345−8349.

(8) Ewald, P. P. *Ann. Phys.* **1921**, *64*, 253−268.

(9) Toukmaji, A. Y.; Jr., J. A. B. *Comput. Phys. Commun.* **1995**, *95*, 73−92.

(10) Deserno, M.; Holm, C. *J. Chem. Phys.* **1998**, *109*, 7678−7693.

(11) Essmann, U.; Perera, L.; Berkowitz, M. L.; Darden, T.; Lee, H.; Pedersen, L. G. *J. Chem. Phys* **1995**, *103*, 8577−8593.

(12) Darden, T.; York, D.; Pedersen, L. *J. Chem. Phys.* **1993**, *98*, 10089−10092.

(13) Shan, Y.; Klepeis, J. L.; Eastwood, M. P.; Dror, R. O.; Shaw, D. E. *J. Chem. Phys.* **2005**, *122*, No. 054101.

(14) Tongraar, A.; Liedl, K. R.; Rode, B. M. *J. Phys. Chem. A* **1998**, *102*, 10340−10347.

(15) Tongraar, A.; Rode, B. M. *J. Phys. Chem. A* **2001**, *105*, 506−510.

(16) Schwenk, C. F.; Loeffler, H. H.; Rode, B. M. *J. Am. Chem. Soc.* **2003**, *126*, 1618−1624.

(17) Chalmet, S.; Ruiz-Lopez, M. F. *J. Chem. Phys.* **2001**, *115*, 5220−5227.

(18) Chalmet, S.; Rinaldi, D.; Ruiz-Lopez, M. F. *Int. J. Quantum Chem.* **2001**, *84*, 559−564.

(19) Bandyopadhyay, P.; Gordon, M. S. *J. Chem. Phys.* **2000**, *113*, 1104−1109.

(20) Gao, J.; Alhambra, C. *J. Chem. Phys.* **1997**, *107*, 1212−1217.

(21) Nam, K.; Gao, J.; York, D. M. *J. Chem. Theory Comput.* **2005**, *1*, 2−13.

(22) Dehez, F.; Martins-Costa, M. T. C.; Rinaldi, D.; Millot, C. *J. Chem. Phys.* **2005**, *122*, No. 234503.

(23) Yarne, D. A.; Tuckerman, M. E.; Martyna, G. J. *J. Chem. Phys.* **2001**, *115*, 3531−3539.

(24) Laino, T.; Mohamed, F.; Laio, A.; Parrinello, M. *J. Chem. Theory Comput.* **2005**, *1*, 1176−1184.

(25) Freely available at the URL http://cp2k.berlios.de, released under GPL license.

(26) Zipoli, F.; Laino, T.; Laio, A.; Bernasconi, M.; Parrinello, M. *J. Chem. Phys.* **2006**, *124*, 154707.

(27) Biswas, P.; Gogonea, V. *J. Chem. Phys.* **2005**, *123*, No. 164114.

(28) *Computer Simulation of Liquids*; Oxford University Press: Oxford, 1987.

(29) VandeVondele, J.; Krack, M.; Mohamed, F.; Parrinello, M.; Chassaing, T.; Hutter, J. *Comput. Phys. Commun.* **2005**, *167*, 103−128.

(30) Lippert, G.; Hutter, J.; Parrinello, M. *Theor. Chem. Acc.* **1999**, *103*, 124−140.

(31) Martyna, G. J.; Tuckerman, M. E. *J. Chem. Phys.* **1999**, *110*, 2810−2821.

(32) Blöchl, P. E. *J. Chem. Phys.* **1995**, *103*, 7422−7428.

(33) Levien, L.; Prewitt, C. T.; Weidner, D. J. *Am. Mineral.* **1980**, *65*, 920−930.

(34) Nelson, C. M.; Weeks, R. A. *J. Am. Ceram. Soc.* **1960**, *43*, 396−399.

(35) Weeks, R. A. *J. Appl. Phys.* **1956**, *27*, 1376−1381.

(36) Weeks, R. A.; Nelson, C. M. *J. Am. Ceram. Soc.* **1960**, *43*, 399−404.

(37) Silsbee, R. H. *J. Appl. Phys.* **1961**, *32*, 1459−1461.

(38) Jani, M. G.; Bossoli, R. B.; Halliburton, L. E. *Phys. Rev. B* **1983**, *27*, 2285−2293.

(39) Warren, W. L.; Poindexter, E. H.; Offenberg, M.; Müller-Warmuth, W. *J. Electrochem. Soc.* **1992**, *139*, 872−880.

(40) Poindexter, E. H.; Warren, W. L. *J. Electrochem. Soc.* **1995**, *142*, 2508−2516.

(41) Hamann, D. R. *Phys. Rev. Lett.* **1996**, *76*, 660−663.

(42) Blöchl, P. E. *Phys. Rev. B* **2000**, *62*, 6158−6179.

(43) Snyder, K. C.; Fowler, W. B. *Phys. Rev. B* **1993**, *48*, 13238−13243.

(44) Allan, D. C.; Teter, M. P. *J. Am. Ceram. Soc.* **1990**, *73*, 3247−3250.

(45) Boero, M.; Pasquarello, A.; Sarnthein, J.; Car, R. *Phys. Rev. Lett.* **1997**, *78*, 887−890.

(46) Pacchioni, G.; Ierano, G. *Phys. Rev. Lett.* **1998**, *81*, 377−380.

(47) Edwards, A. H.; Fowler, W. B. *J. Phys. Chem. Solids* **1985**, *46*, 841−857.

(48) Rudra, J. K.; Fowler, W. B. *Phys. Rev. B* **1987**, *35*, 8223−8230.

(49) Pacchioni, G.; Ferrari, A. M.; Ierano, G. *Faraday Discuss.* **1997**, *107*, 155−172.

(50) Sauer, J.; Sierka, M. *J. Comput. Chem.* **2000**, *21*, 1470−1493.

(51) Sulimov, V.; Sushko, P. A. H.; Edwards, A. S.; Stoneham, A. *Phys. Rev. B* **2002**, *66*, 24108−24114.

(52) Mysovsky, A.; Sushko, P.; S. Mukhopadhyay, A. E.; Shluger, A. *Phys. Rev. B* **2004**, *69*, No. 085202.

(53) Sulimov, V.; Casassa, S.; Pisani, C.; Garapon, J.; Poumellac, B. *Modell. Simul. Mater. Sci. Eng.* **2000**, *8*, 763−773.

(54) Pisani, C.; Busso, M.; Lopez-Gejo, F.; Casassa, S.; Maschio, L. *Theor. Chem. Acc.* **2004**, *111*, 246−254.

(55) Erbetta, D.; Ricci, D.; Pacchioni, G. *J. Chem. Phys.* **2000**, *113*, 10744−10752.

(56) Nasluzov, V.; Ivanova, E.; Shor, A.; Vayssilov, G.; Birkenheuer, U.; Rosch, N. *J. Phys. Chem. B* **2003**, *107*, 2228−2241.

(57) van Beest, B. W. H.; Kramer, G. J.; van Santen, R. A. *Phys. Rev. Lett.* **1990**, *64*, 1955−1958.

(58) Tse, J.; Klug, D. D.; Page, Y. L. *Phys. Rev. B* **1992**, *46*, 5933−5938.

(59) Goedecker, S.; Teter, M.; Hutter, J. *Phys. Rev. B* **1996**, *54*, 1703−1710.

(60) Phillipp, H. R. *Solid State Commun.* **1966**, *4*, 73−75.

(61) Miyazaki, S.; Nishimura, H.; Fukuda, M.; Ley, L.; Ristein, J. *Appl. Surf. Sci.* **1997**, *113/114*, 585−589.

(62) *The Feynman Lectures on Physics*; Addison-Wesley: 1963; Vol. 1, pp 30−11.

CT6001169